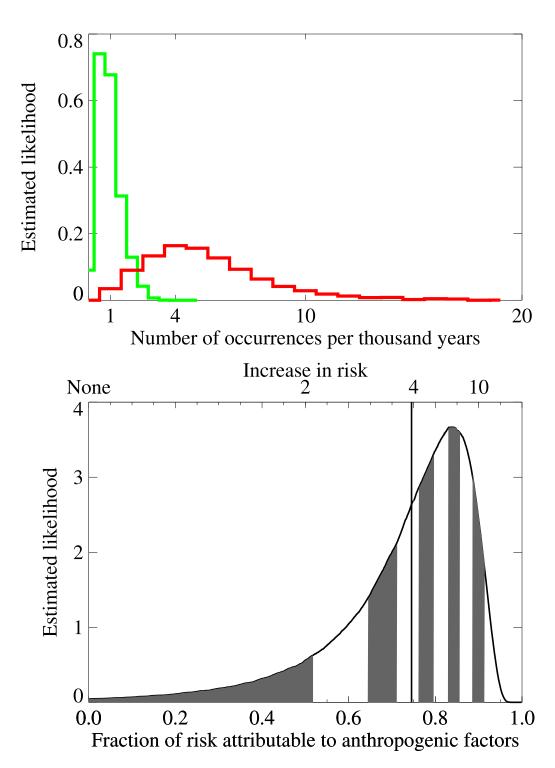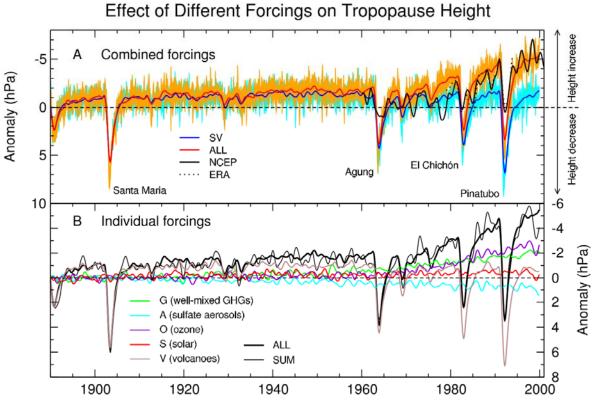**Figure 9.4.8.** Comparison of IPCC AR4 C20C3M model simulations containing all forcings (red shaded regions) and IPCC AR4 C20C3M model simulations containing natural forcings only (blue shaded regions) with the observed (HadCRUT2v, Parker et al., 2004) decadal mean temperature changes in 1906–2005 at bottom left for global mean (GLO), global land (LAN) and global ocean (OCE) and, 22 sub-continental scale regions (defined in Chapter 11, Giorgi and Francisco, 2000) positioned over the geographical region they represent for North America regions (ALA, CGI, WNA, CNA, ENA), Central and South America regoins (CAM, AMZ, SSA), Europe regions (NEU,SEU), Africa regions (SAH, WAF, EAF, SAF), Asia regions (NAS, CAS, TIB, EAS, SAS, SEA) and Australia regions (NAU, SAU). Shaded bands represent the 5 to 95 percentile range estimated from the multi-model ensemble. Note that the model simulations have not been scaled in any way. The same simulations used are as in Figure 9.4.1 (51 all forcings simulations from 13 models, and 19 natural forcings only simulations from 5 models). Each simulation was sampled so that coverage corresponds to that of the observations, and was centered relative to the 1901–1997 mean obtained by that simulation in the region of interest. Observations in each region were centered relative to the same period. The observations in each region are generally consistent with model simulations that include anthropogenic and natural forcings, whereas in many regions the observations are inconsistent with model simulations that include natural forcings only.

1
2

Figure 9.4.9. Change in risk of mean European summer temperatures exceeding a threshold of 1.6°C above 1961–1990 mean temperatures, a threshold that was exceeded in 2003 but in no other year since the start of the instrumental record in 1851. a) Frequency histograms of threshold exceedence under late-twentieth-century conditions in the absence of anthropogenic climate change (green line) and with anthropogenic climate change (red line). b) Fraction of attributable risk (FAR). Also shown, as the vertical line, is the "best estimate" FAR, the mean risk attributable to anthropogenic factors averaged over the distribution. The alternation between grey and white bands indicates the deciles of the estimated FAR distribution. From Stott et al. (2004).

1
2

Santer et al. Figure 1A,B

3
4
Figure 9.4.10. Time series of global mean monthly mean anomalies in tropopause pressure (pLRT). Model
results are from seven different PCM (model ID 21, Chapter 8, Table 8.2.1) ensemble experiments. Five
experiments use a single forcing only (G, A, O, S, or V). Two integrations involve combined forcing
changes, either in natural forcings (SV), or in all forcings (ALL). There are four realizations of each
experiment. In B, only low-pass filtered ensemble means are shown. In A both the low-pass filtered
ensemble mean and the (unfiltered) range between the highest and lowest values of the realizations are
given. All model anomalies are defined relative to climatological monthly means computed over 1890–1999.
Reanalysis based pLRT estimated from NCEP and ERA were filtered in the same way as model data. NCEP
pLRT data are available from 1948–2001, but pre-1960 data were ignored because of deficiencies in the
coverage and quality of assimilated radiosonde data. The ERA record spans 1979–1993. NCEP (ERA) was
forced to have the same mean as ALL over 1960–1999 (1979–1993). The SUM results (B) are the sum of the
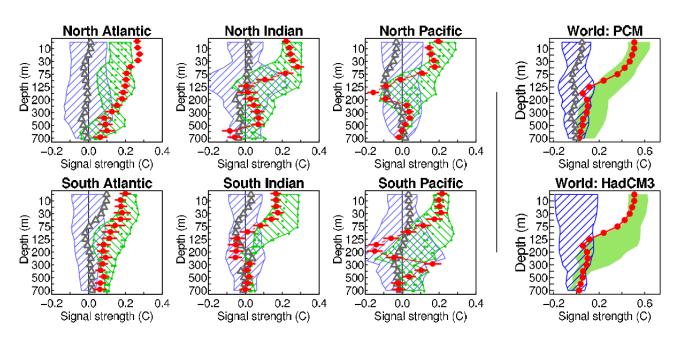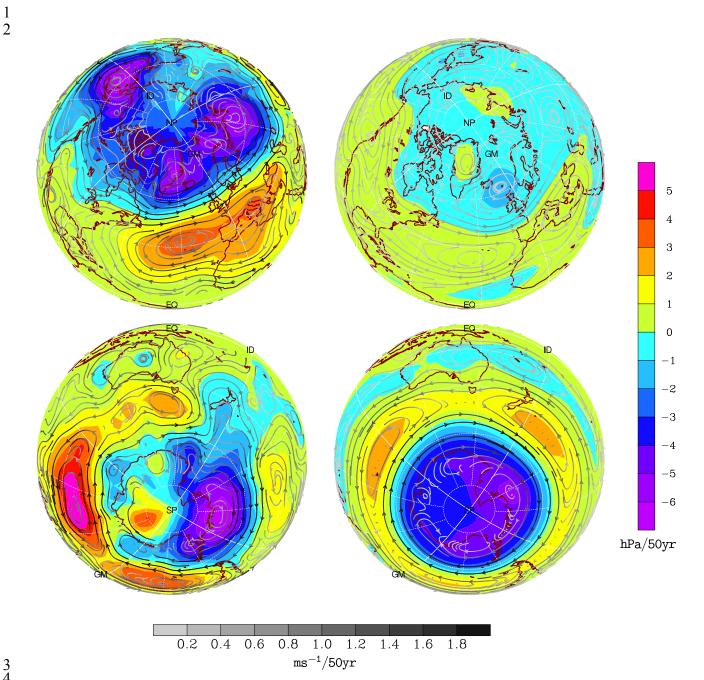filtered ensemble-mean responses from G, A, O, S, and V. From Santer et al. (2003a).

17

1
2

3
4
5 **Figure 9.5.1.** Warming signal strength by depth for the world ocean and for each ocean basin individually.
6 For ocean basins the signal is estimated from PCM (model ID 21, Chapter 8, Table 8.2.1) while it is
7 estimated from both PCM and HadCM3 (model ID 22, Chapter 8, Table 8.2.1) for the world ocean. Red dots
8 represent the projection of the observed temperature changes onto the model-based pattern of warming. They
9 show substantial basin-to-basin differences in how the oceans have warmed over the past 40 years, although
10 all oceans have experienced net warming over that interval. The red bars represent the ± two standard
11 deviations limits associated with sampling uncertatinty. The blue cross hatched swaths represent the 90%
12 confidence limits of the natural internal variability strength. The green cross hatched swaths represent the
13 range of the anthropogenically forced signal estimates from different realizations of identically forced
14 simulations with the PCM model for each ocean basin (the smaller dots within the green swaths are the
15 individual realizations) and the green shaded regions represent the range of anthropogenically forced signal
16 estimates from different realizations of identically forced simulations with the PCM and HadCM3 models
17 for the world ocean (note that PCM and HadCM3 contain different represenations from each other of
18 anthropogenic forcings). The ensemble averaged strength of the warming signal in four PCM simulations is
19 also shown (grey triangles). From Barnett et al. (2005) and Pierce et al. (2006).
20

1
2

3
4
Figure 9.5.2. December-February sea-level pressure trends based on decadal means for the period 1955–
2005 are shown for HadSLP2r (an infilled observational dataset) (left) , and the mean simulated response to
greenhouse gas, sulphate aerosol, stratospheric ozone, volcanic aerosol, and solar irradiance changes in eight
IPCC AR4 coupled models (CCSM3, GFDL-CM2.0, GFDL-CM2.1, GISS-EH, GISS-ER,
MIROC3.2(medres), PCM, UKMO-HadCM3; model IDs 3, 11, 12, 14, 15, 19, 21 and 22, Chapter 8, Table
8.2.1) (right). Streamlines indicate the direction of the trends in the geostrophic wind derived from the trends
in sea-level pressure, and the shading of the streamlines indicates the magnitude of the change, with darker
streamlines corresponding to larger changes in geostrophic wind. Units: hPa/ 50 yr (SLP), m/s/ 50 yr (wind
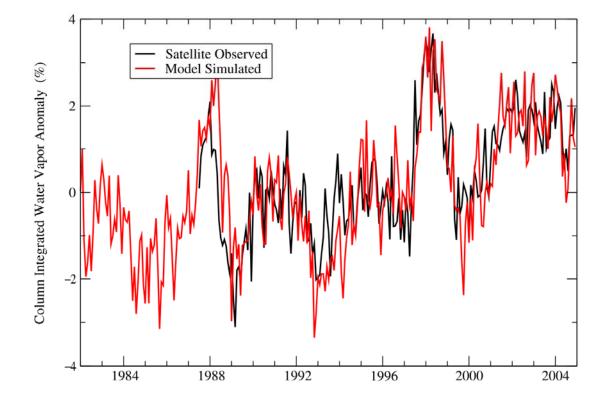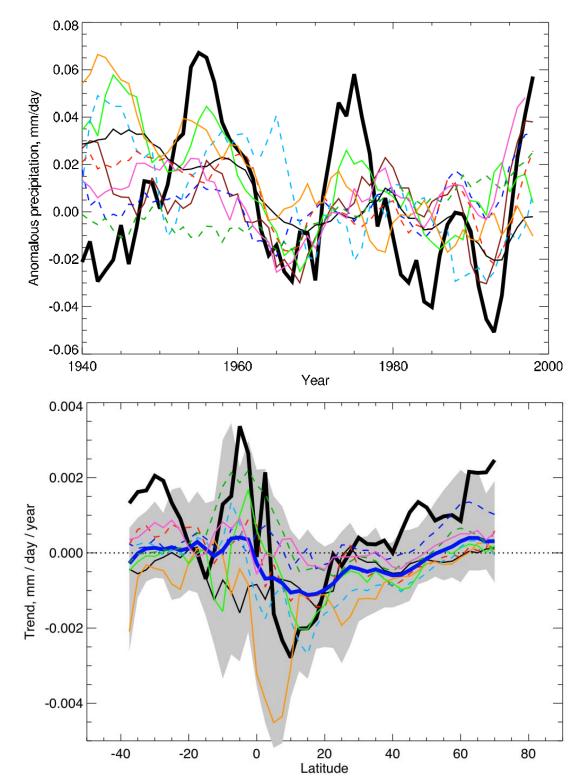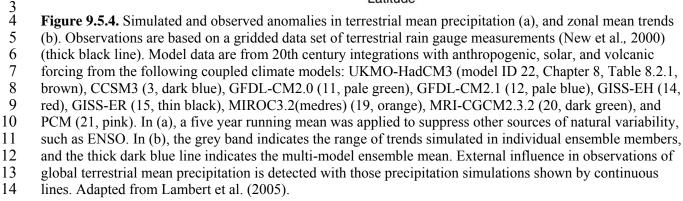velocity). Based on Gillett et al. (2005).
14

1
2

3
4 **Figure 9.5.3.** Global mean (ocean-only) anomalies in column integrated water vapour from simulations with
5 the Geophysical Fluid Dynamics Laboratory (GFDL) AM2-LM2 atmospheric GCM forced with observed
6 sea surface temperatures (red), and satellite observations from SSMI (black, Wentz and Schabel, 2000)).
7 From Soden et al. (2005).
8

1

2

3
4   **Figure 9.5.4.** Simulated and observed anomalies in terrestrial mean precipitation (a), and zonal mean trends
5   (b). Observations are based on a gridded data set of terrestrial rain gauge measurements (New et al., 2000)
6   (thick black line). Model data are from 20th century integrations with anthropogenic, solar, and volcanic
7   forcing from the following coupled climate models: UKMO-HadCM3 (model ID 22, Chapter 8, Table 8.2.1,
8   brown), CCSM3 (3, dark blue), GFDL-CM2.0 (11, pale green), GFDL-CM2.1 (12, pale blue), GISS-EH (14,
9   red), GISS-ER (15, thin black), MIROC3.2(medres) (19, orange), MRI-CGCM2.3.2 (20, dark green), and
10   PCM (21, pink). In (a), a five year running mean was applied to suppress other sources of natural variability,
11   such as ENSO. In (b), the grey band indicates the range of trends simulated in individual ensemble members,
12   and the thick dark blue line indicates the multi-model ensemble mean. External influence in observations of
13   global terrestrial mean precipitation is detected with those precipitation simulations shown by continuous
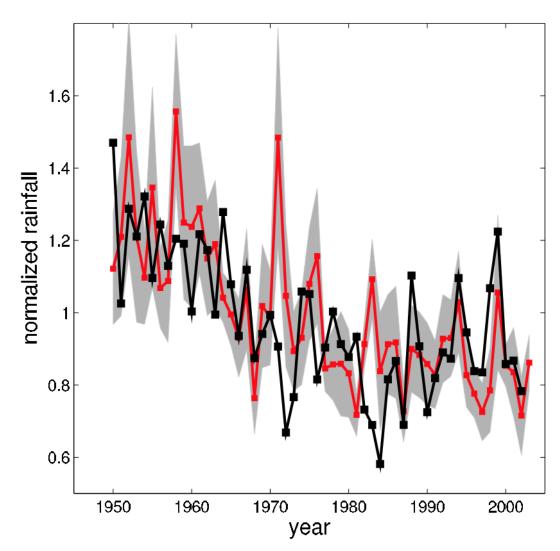14   lines. Adapted from Lambert et al. (2005).

1
2

3
4
5   **Figure 9.5.5.** Observed (CRU-TS2.1, Mitchell and Jones, 2005) Sahel July-September rainfall for each year
6   (black), and an ensemble mean of 10 simulations of the atmospheric/land component of GFDL-CM2.0
7   model forced with observed sea surface temperatures (red). The grey band represents ± one standard
8   deviation of intra-ensemble variability. From Held et al. (2005).
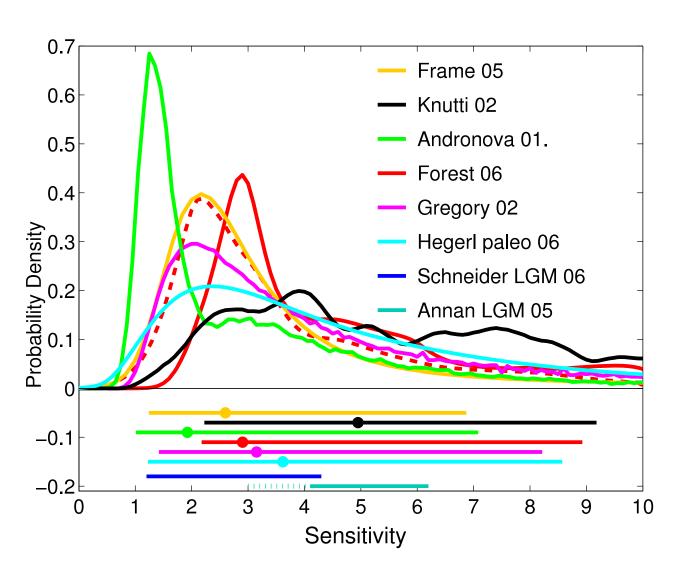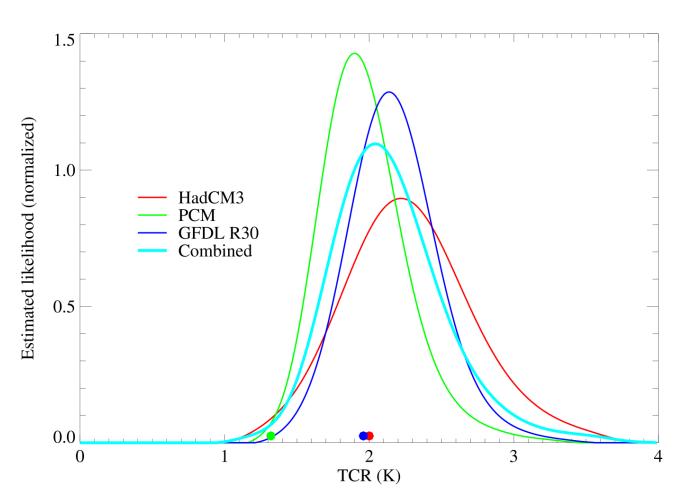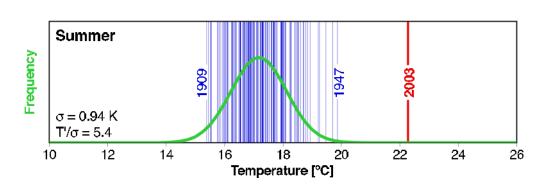9

1
2

3
4
Figure 9.6.1. Comparison between different estimates of the probability density function (or relative
likelihood) for equilibrium climate sensitivity. All PDFs/likelihoods have been scaled to integrate to 1
between 0 and 10. The bars show the respective 5–95% ranges, dots the median estimate. Pdfs/likelihoods
based on instrumental data are from Andronova and Schlesinger (2001), Forest et al. (2002) (dashed line,
considering anthropogenic forcings only), Forest et al. (2006) (solid, anthropogenic and natural forcings),
Gregory et al. (2002a), Knutti et al. (2002), Frame et al. (2005). Hegerl et al. (2006) is based on paleo
reconstructions of temperatures in the last 700 years. Also shown are the 5–95% approximate ranges for two
estimates from the Last Glacial Maximum (dashed, Annan et al., 2005; solid, Schneider von Deimling et al.,
2006) which are based on models with different structural properties. Note that the latter range is extended
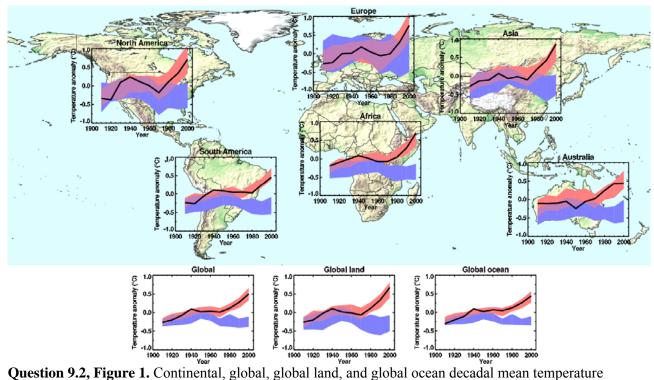by dots towards lower sensitivities than sampled by their model.
15

1
2

3
4
Figure 9.6.2. Probability distributions of transient climate response (TCR, expressed as warming rates over
the century), as constrained by observed 20th century temperature change, for HadCM3 (model ID 22,
Chapter 8, Table 8.2.1, red), PCM (21, green), GFDL R30 (Delworth et al., 2002, blue) models and
averaging the PDFs derived from each model (turquoise). Coloured stars show each model's TCR. (From
Stott et al., 2006c).

10

1
2

3
4
5 **Question 9.1, Figure 1.** Distribution of Swiss seasonal summer temperatures for 1864–2003. The fitted
6 Gaussian distribution is indicated in green. The values in the lower left corner indicate the standard deviation
7 (σ) and the 2003 anomaly normalized by the 1864–2000 standard deviation (T'/ σ). From Schär et al. (2004).
8

1
2

3
4 **Question 9.2, Figure 1.** Continental, global, global land, and global ocean decadal mean temperature
5 anomalies for 1906–2005 relative to the period 1901–1997. Observed (black, HadCRUT2v, Parker et al.,
6 2004). Red, approximate 5–95% range of IPCC AR4 simulations of the 20th century using anthropogenic
7 and natural forcings. The red band was determined from 51 simulations from 13 models that did not exhibit
8 excessive drift in their control simulations (no more than 0.2ºC per century). Thirteen models are included;
9 11 of which are described in Chapter 8, Table 8.2.1 and are identified in the list below by their Model ID
10 given in that table. An additional two models are not described in Chapter 8, Table 8.2.1; these are
11 ECHAM4-OPYC3 (Stendel et al., 2006), and GFDL-R30 (Delworth et al., 2002). Model simulations
12 including both anthropogenic and natural forcings are: CCSM3 (model ID 3; 6 simulations), ECHO-G (9,3),
13 GFDL-CM2.0 (11,3), GFDL-CM2.1 (12,3), GFDL-R30 (A2, 3), 6: GISS-EH (14,5), 7: GISS-ER (15,9), 8:
14 INM-CM3.0 (16,1), 9: MIROC3.2(medres) (19,4), 10: MRI-CGCM2.3.2 (20,5), 11: PCM (21,4), 12:
15 HadCM3 (22,4). Model simulations including natural forcings only are: ECHO-G (model ID 9;3
16 simulations), MIROC3.2(medres) (19,4), MRI-CGCM2.3.2 (20,4), PCM (21,4), HadCM3 (22,4). Each
17 simulation was sampled so that coverage corresponds to that of the observations, and was centered relative to
18 the 1901-1997 mean obtained by that simulation in the region of interest. The blue band was determined
19 similarly from 19 simulations from 5 models using only natural forcings. Model simulations including
20 natural forcings only are: ECHO-G (model ID 9, 3 simulations), MIROC3.2(medres) (19,4), MRI-
21 CGCM2.3.2 (20,4), PCM (21,4), HadCM3 (22,4).
22